JOURNAL OF GUIDANCE, CONTROL, AND DYNAMICS
Vol. 32, No. 2, March–April 2009

Flight Trajectory Optimization to Minimize Ground Noise in Helicopter Landing Approach

Takeshi Tsuchiya*
University of Tokyo, Tokyo 113-8656, Japan
Hirokazu Ishii†
Japan Aerospace Exploration Agency, Tokyo 182-8522, Japan
Junichi Uchida‡ and Hiroshi Ikaida‡
University of Tokyo, Tokyo 113-8656, Japan
and
Hiromi Gomi,§ Naoki Matayoshi,¶ and Yoshinori Okuno§
Japan Aerospace Exploration Agency, Tokyo 182-8522, Japan

DOI: 10.2514/1.34458

The purpose of this paper is to optimize helicopter flight trajectories to reduce ground noise in the landing approach using an optimization technique and to conduct flight experiments to confirm the effectiveness of the optimal solutions. The Japan Aerospace Exploration Agency has thus far measured helicopter noise under various flight conditions. This study builds a noise model of the helicopter in which the level of noise generated from a point noise source is a function of the flight path angle and bank angle. Then, we define optimal control problems that minimize the noise levels measured at points on the ground surface using equations of motion of 3 degrees of freedom for three-dimensional flight, and obtain the optimal controls for some flight constraints and wind conditions. The obtained optimal flights avoid the flight path angle that generates a great deal of noise and skirt the measurement points; these optimal flights are different from the conventional flight. Finally, this study verifies the validity of the optimal flight patterns by means of flight experiments with an experimental Japan Aerospace Exploration Agency helicopter. The actual flights following the optimal flights result in noise reduction and prove the effectiveness of the optimization.

Nomenclature

att	=	total noise attenuation
att_{air}	=	atmospheric absorption of noise
att_{dist}	=	noise attenuation by distance
E_A	=	energy-based noise estimation
g	=	acceleration due to gravity (32.174 ft/s^2)
h	=	altitude
J	=	performance index
L	=	noise level
L_A	=	temporal-mean noise level
L_i	=	noise level at measurement point i
L_m	=	measurement-point mean noise level
L_{ref}	=	reference noise level (noise level measured at reference distance r_{ref})
m	=	mass
r	=	distance to helicopter
r_i	=	distance from measurement point i to helicopter
r_{ref}	=	reference distance at which the noise level L_{ref} is measured
S_u	=	square integration of variation of control values
T	=	thrust
t	=	time
t_f	=	final time
U	=	horizontal velocity
u_g	=	wind speed
W	=	climb rate
w	=	weight factor for S_u in the performance index
x	=	position of helicopter (x coordinate)
y	=	position of helicopter (y coordinate)
γ	=	flight path angle
Θ	=	pitch angle
Φ	=	roll angle
ψ	=	heading angle
ψ_g	=	wind direction

Received 6 September 2007; revision received 2 October 2008; accepted for publication 12 October 2008.

*Associate Professor, Department of Aeronautics and Astronautics; tsuchiya@mail.ecc.u-tokyo.ac.jp. Member AIAA.
†Researcher, Operation and Safety Technology Team, Aviation Program Group; ishii.hirokazu@jaxa.jp. Member AIAA.
‡Graduate Student, Department of Aeronautics and Astronautics.
§Senior Researcher, Operation and Safety Technology Team, Aviation Program Group.
¶Researcher, Operation and Safety Technology Team, Aviation Program Group.

I. Introduction

BECAUSE helicopters are different from fixed-wing aircraft in that the helicopters do not require a large runway during takeoff and landing and have high maneuverability, they are relied upon as an effective means of transport in suburban and mountainous areas. They have been used for missions such as news reporting or disaster and rescue emergencies. However, a major problem in helicopter operations is noise. The large noise that spreads throughout the environment surrounding a flight path is arguably one of the main reasons that helicopters are not used more widely. While noise originates from points throughout the helicopter, for example, the rotor, engine, and transmission, one particular type of noise, which is known as blade-vortex interaction (BVI) noise, occurs during landing and flight at low altitude. BVI noise occurs when the wingtip vortices emitted at the main rotor blades interfere with other blades. Because the magnitude, which varies with flight conditions, is large especially during descent flight, the landing approach at low altitude produces a large amount of noise damage to the environment. In addition, because the selection of a flight path is basically entrusted to the pilot judgment, the amount of noise affecting densely populated

areas depends on the pilots experience. However, because the propagation characteristics of helicopter noise change due to factors such as climate conditions, the actual noise at the ground surface is not necessarily consistent with the noise experienced by the pilot. In particular, it is likely that serious noise damage can occur in areas where the pilot does not know the landscape. Thus, in the future, it will be necessary to reduce the damage by dispersing the noise over tolerant areas such as rivers, commercial regions, or forests using a precision approach system.

Based on the background described above, the Federal Aviation Administration (FAA), National Aeronautics and Space Administration (NASA), and universities in the United States have performed advanced research involving numerical models of helicopter and aircraft noise. The integrated noise model developed by the FAA, which uses a simple model expressing an aircraft as a point sound source of its noise, is in broad use at flight operation sites around the world. NASA has studied the BVI noise reduction of rotorcrafts through flight trajectory management. In particular, NASA, Bell Helicopter Textron Inc., and the U.S. Army have conducted a collaborative study on noise abatement flight of the XV-15 tiltrotor aircraft [1]. Xue and Atkins of the University of Maryland determined the noise-minimum approach trajectory for a specific airport considering the population density around the airport [2]. The flight trajectory was, however, simplified to facilitate optimization. In Europe, the research project, SILENCER, has developed noise-reduced aircraft. The German Aerospace Center (Deutsche Forschungsanstalt für Lüft und Raumfahrt, DLR) and the Delft University of Technology have conducted studies on flight trajectory optimization to reduce noise. DLR simulated the ground noise of a helicopter and compared it with flight test data [3]. In [4], the Delft University of Technology optimized the departure and approach trajectories of more than one aircraft, but no comparison with flight test data was made.

In Japan, the Japan Aerospace Exploration Agency (JAXA) has also developed a system to estimate and display the ground-level noise damage caused by a helicopter in real time on board the vehicle [5]. JAXA has performed advanced studies on methods for measuring noise using actual aircraft and has measured the noise at ground level and on board an experimental helicopter, the MuPAL-ε (Fig. 1) [6,7]. Researchers at JAXA have also calculated rotor noise using computational fluid dynamics (CFD) [8]. The computational accuracy of CFD has increased with advances in computational techniques and computing power, and CFD has been applied to studies of noise reduction through improvements in blade shape. However, it is not possible to estimate noise impact for actual flights in real time with the current computing power. The first author of this paper has studied numerical solution methods of optimal control problems at the University of Tokyo. That study aimed at an optimization algorithm that would be applicable to actual existing problems with relatively high versatility [9]. With this background, JAXA and the University of Tokyo are currently pursuing collaborative research regarding landing approach trajectories that minimize helicopter noise damage. The present study focuses on the fact that the noise emanating from a helicopter depends on flight conditions and aims to reduce the ground-level noise damage by optimizing the landing approach flight path using numerical computation methods. Our preceding paper [10] considered the vertical motion of the helicopter, that is, the altitude and velocity control, for the sake of simplicity. This paper defined a two-dimensional optimal control problem for minimizing noise levels measured on the ground surface, obtained optimal controls, and then verified the validity of the optimal controls by means of flight experiments.

This paper modifies the noise model and the attenuation model from the results of [10]. In addition, a three-dimensional optimal control problem in which the helicopter can engage in three-dimensional flight is defined, whereas [10] limited the motion to two dimensions. The main objective of this paper is to verify the validity of these models. A further objective is to confirm, during flight tests using MuPAL-ε, effective noise abatement of flight paths based on the optimal solutions. This paper first outlines the flight test environment and conditions. Optimal control problems are then defined accordingly, and the results of computational optimization are shown. Thereafter, this paper presents the results of the flight tests. Finally, our conclusions are explained.

Fig. 1 The JAXA experimental helicopter, MuPAL-ε.

II. Flight Test Environment and Conditions

In preparation for the definition of optimal control problems in the next section, this section summarizes the flight test environment and conditions in which the results of the optimal controls are experimentally validated. The optimal control problems are defined according to the environment.

This study used the multipurpose aviation laboratory MuPAL-ε of JAXA as a flight experimental helicopter (Fig. 1) [6,7]. MuPAL-ε, which is based on the Mitsubishi MH2000A, is equipped with a precision data acquisition system, programmable cockpit displays, and other experimental support systems. A pilot can manually control the helicopter following a 3-D guidance system displayed on the cockpit instrument panel. This system was used for the flight test. The flight tests were carried out in the vicinity of the Taiki multipurpose aeronautical park at a latitude of 42.50° north and a longitude of 143.44° east in Japan. JAXA frequently conducts large-scale flight experiments in the Taiki multipurpose aeronautical park because it is far from airline flight paths and has steady weather and a 1000 m paved runway. The reference flight path for approaching the runway was determined with consideration given to establishing a low-noise environment and the ease of installing noise measurement devices. For example, areas with a lot of traffic were avoided. Five noise measurement points are set around the reference flight path. The north–east–down (NED) coordinate system with a supposed landing point as the origin was defined. Figure 2 shows a map of the area around the reference path and measurement points. Table 1 indicates the coordinates of the noise measurement points. The coordinates of the helicopter's initial point at the moment it began the

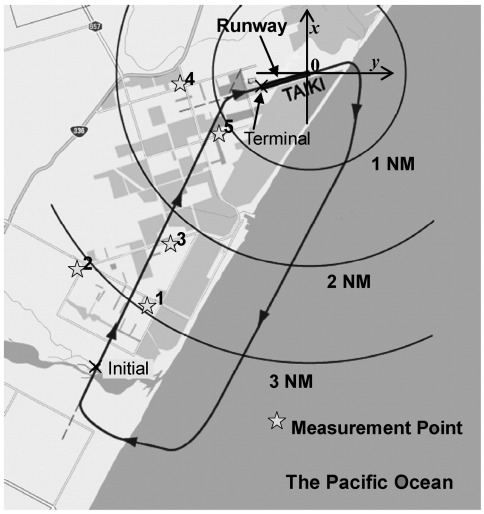

Fig. 2 A reference path and five measurement points around the Taiki multipurpose aeronautical park. (NM = n mile.)

Table 1 The coordinates of measurement points

No. of measurement points	x, n mile	y, n mile
1	−2.37	−1.66
2	−2.00	−2.38
3	−1.74	−1.40
4	−0.15	−1.33
5	−0.64	−0.87

landing approach were set to $(x,\ y) = (-2.987,\ -2.186)$ (n mile), and the altitude at that time was approximately 1850–2300 ft. The initial heading angle was 23.36 deg. The coordinates of the terminal point were $(x,\ y) = (-0.136,\ -0.45)$ (n mile), with an altitude of 300 ft. The terminal heading angle was 73.20 deg. Because the final maneuvering from the terminal point at an altitude of 300 ft to landing on the ground was left to the pilot of the helicopter, it was outside the scope of the optimal controls in this paper. The terminal position was defined on the extension line in the runway, and the terminal heading angle was identical to the runway angle so that horizontal maneuvering was not required at an altitude of less than 300 ft. The helicopter flew over the measurement points from the initial point to the terminal point using proper altitude, speed, and roll controls. The problem of this study was to find a flight pattern minimizing the noise levels measured at the five measurement points.

III. Optimal Controls

A. Definition of Optimal Control Problems

To derive the helicopter equations of motion used in this paper, the helicopter was treated as a point mass. The equations of motion were as follows.

$$\dot{x} = U\cos\psi - u_g\cos\psi_g \tag{1}$$

$$\dot{y} = U\sin\psi - u_g\sin\psi_g \tag{2}$$

$$\dot{h} = W \tag{3}$$

$$\dot{U} = -\frac{T}{m}\cos\Phi\sin\Theta \tag{4}$$

$$\dot{W} = -g + \frac{T}{m}\cos\Phi\cos\Theta \tag{5}$$

$$\dot{\psi} = \frac{T}{mU}\sin\Phi \tag{6}$$

The vertical position of the helicopter was expressed in terms of the altitude h instead of the z axis that is downward positive in the NED coordinate system. The six state variables were controlled by the three variables: the thrust T, pitch angle Θ, and roll angle Φ. It was assumed that the mass m did not change while flying. These equations of motion included only two external forces acting on the helicopter: the thrust of the main rotor and gravity. Aerodynamic forces were ignored because there is no sense of including the aerodynamic forces in the motion equations. As mentioned below, there are acceleration limits but not thrust constraints. Thus, even if the equations included the aerodynamic forces, the thrust necessary to overcome the aerodynamic forces could be provided. The computation results will show that the thrust is kept within a permissible range even without the thrust constraints. Though the added thrust results in added noise, the noise source in this paper includes such an effect. There is no need for the added noise. That is why Eqs. (1–6) do not include the aerodynamic forces. The equations included a horizontal and constant wind with the wind velocity u_g and wind direction ψ_g, independent of altitude or time. Possible wind speeds and directions in the flight environment for u_g and ψ_g are substituted. The value for u_g is from −20 to 20 kt, and the value of ψ_g is 31.34 deg or −58.66 deg, as indicated in Sec. III.E.

Next the initial and terminal conditions of the optimal control problems were defined. The initial conditions at $t = 0$ were related to the state when the landing approach begins, which were explained in the previous section,

$$x(0) = -2.987 \text{ n mile} \tag{7}$$

$$y(0) = -2.186 \text{ n mile} \tag{8}$$

$$h(0) = \text{free} \tag{9}$$

$$U(0) = 100 \text{ kt} \tag{10}$$

$$W(0) = 0 \text{ ft/min} \tag{11}$$

$$\psi(0) = 26.36 \text{ deg} \tag{12}$$

When the flight began, the helicopter flew horizontally and the airspeed was set to 100 kt. The initial altitude $h(0)$ was not specified but optimized. The terminal conditions at $t = t_f$ indicated completion of the landing approach flights. As described in the previous section, the following is defined:

$$x(t_f) = -0.136 \text{ n mile} \tag{13}$$

$$y(t_f) = -0.450 \text{ n mile} \tag{14}$$

$$h(t_f) = 300 \text{ ft} \tag{15}$$

$$U(t_f) = 50 \text{ kt} \tag{16}$$

$$W(t_f) = -500 \text{ ft/min} \tag{17}$$

$$\psi(t_f) = 73.20 \text{ deg} \tag{18}$$

The final time t_f was also an optimized parameter.

In addition, the constraint conditions during flight were defined. The helicopter motion was calculated using the above-mentioned simple model, but the actual helicopter was controlled by the pilot manually during the flight experiments. It was therefore necessary for the pilot to follow the optimal solutions without being burdened by an excessive workload. An experiment using a flight simulator owned by JAXA was performed to determine the constraint conditions, and then settled upon the four types of constraint conditions listed next.

1) Horizontal-velocity limit,

$$50 \le U \le 100 \text{ kt} \tag{19}$$

2) Climb-rate limit.

Considering the psychological impact on the pilot of taking a steep dive at low altitude, the constraint conditions were differentiated by altitude to establish a relatively strict limit below 480 ft.

When $h \geq 480$ ft,

$$|W| \leq 800 \text{ ft/min} \tag{20}$$

When $h \leq 480$ ft,

$$-\left(\frac{h}{480}\right)800 \leq W \leq 800 \text{ ft/min} \tag{21}$$

However, in an optimization case, the upper limit on the climb rate is replaced with

$$W \leq 0 \tag{22}$$

so the helicopter will descend consistently in the landing approach. The details are discussed later.

3) Acceleration limit

$$|\dot{U}| \leq 1.5 \text{ kt/s} \tag{23}$$

$$|\dot{W}| \leq 100 \text{ ft/min/s} \tag{24}$$

4) Roll angle limit

$$|\Phi| \leq 15 \text{ deg} \tag{25}$$

B. Noise Source Model

Helicopter noise emanates from various sources such as the rotor, engine, and gearbox. In addition, the frequency and directivity depend on the flight conditions. JAXA has measured the noise level of MuPAL-ε by various methods [6,7]. Ishii et al. [6,7] show that the noise, especially BVI noise, varies with change in the flight path angle and airspeed and has the directivity of radiation. However, a characteristic of the noise of MuPAL-ε is that the change caused by the airspeed is smaller than the flight path angle. Moreover, though it was possible to introduce a noise source model including the directivity, this paper investigated the applicability of a simple noise source model for our first study. Therefore, the directivity was ignored. This research used the noise source model of MuPAL-ε which depends on the flight path angle $\gamma\,(=\tan^{-1}W/U)$ and the roll angle Φ. The noise is largest around a flight path angle of -5 deg. An ascent flight that requires large engine torque generates a large noise. In addition, the noise level depends on the roll angle because flight with a large roll angle also requires large engine torque. These characteristics give a simplified noise source model with a reference noise level L_{ref} as shown in Fig. 3. The noise levels in Fig. 3 compensate for human hearing using A weighting and were converted to the level measured at a distance of 100 m from the helicopter (reference distance r_{ref}). The noise level L_{ref} is expressed in terms of the following equations. When $\gamma < -15$ deg or 5 deg $< \gamma$,

$$L_{\text{ref}}(\gamma,\ \Phi) = 81.5 + 0.1\gamma - 80\log(\cos\Phi) \text{ (dB)} \tag{26}$$

When -15 deg $\leq \gamma \leq 5$ deg,

$$L_{\text{ref}}(\gamma,\ \Phi) = 84.5 + 3\cos\left(\frac{\gamma+5}{10}\pi\right) + 0.1\gamma - 80\log(\cos\Phi) \text{ (dB)} \tag{27}$$

C. Attenuation Model

The noise emitted from the helicopter is subject to the influence of various factors during its propagation to ground level, such as the inverse square law of distance, atmospheric damping, ground-surface damping, wind, air temperature, and humidity. This paper considers two types of attenuation: the simple inverse square law of distance and atmospheric absorption. For the inverse square law of distance, the attenuation $\text{att}_{\text{dist}}(r)$ at a point with a distance r from the noise source is

$$\text{att}_{\text{dist}}(r) = 20\log\frac{r}{r_{\text{ref}}} \text{ (dB)} \tag{28}$$

Incorporating atmospheric absorption is more complicated. The relation between the distance and overall noise level depends on the frequency characteristics of the noise source, because the atmospheric absorption depends on frequency. Therefore, the noise level at each frequency was calculated and the energy of the noise was summed to obtain the atmospheric absorption $\text{att}_{\text{air}}(r)$ in all frequency ranges. Figure 4 shows the relation between $\text{att}_{\text{air}}(r)$ and the distance r from MuPAL-ε. The above-mentioned attenuations are combined to compute $\text{att}(r)$,

$$\text{att}\,(r) = \text{att}_{\text{dist}}(r) + \text{att}_{\text{air}}(r) \text{ (dB)} \tag{29}$$

According to Eqs. (26), (27), and (29), at time t, the noise level $L(t)$ measured at a distance $r(t)$ from the helicopter flying with a flight path angle $\gamma(t)$ and roll angle $\Phi(t)$ is calculated as

$$L(t) = L_{\text{ref}}(\gamma(t), \quad \Phi(t)) - \text{att}(r(t)) \text{ (dB)} \tag{30}$$

This study ignored the time needed for the noise to propagate from the noise source to the measurement point. The noise source model and attenuation model indicated herein are simple. However, the excessive complication of these models increases the computation cost and might worsen the convergence due to nonlinearity. As mentioned above, this paper first investigated the applicability of the simple noise model. By comparing the results of the computational optimization with flight test results, the validity of the proposed noise source model and attenuation model was confirmed. As shown below in this paper, the experiments indicated that the noise model has sufficient accuracy to catch the trend.

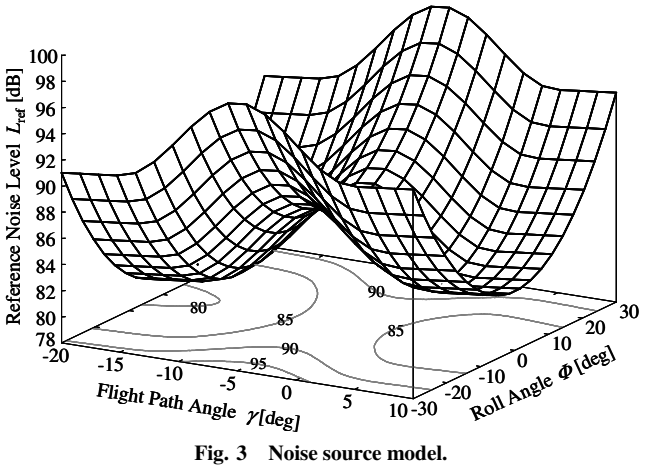

Fig. 3 Noise source model.

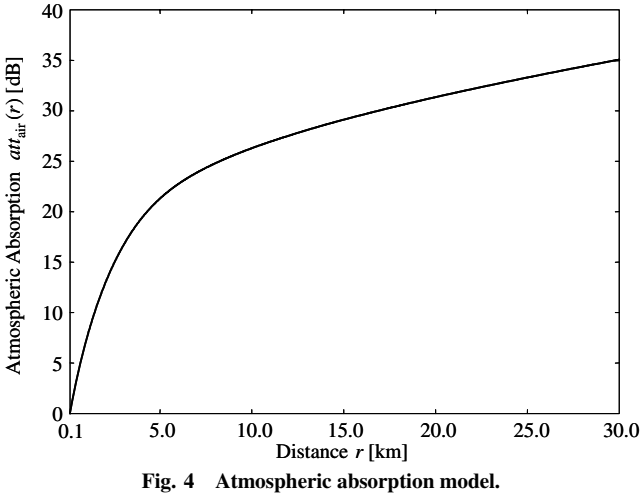

Fig. 4 Atmospheric absorption model.

D. Performance Index

Although the level of the helicopter noise measured at a point on the ground was estimated objectively as described in the previous section, determining how unpleasant the experience is for a person is a subjective problem. That is to say, noise estimation must reflect the degree of influence the noise has on human psychology and physiology, but on the other hand it must be able to be measured objectively. This study therefore used an energy-based noise estimation that is widely used for aircraft noise estimation as a noise estimation index [11]. This index is computed by time integrating the energy of the noise level at each instant. The problem is that there were multiple measurement points in this study. First, the noise level $L_i(t)$ of the measurement point i ($i = 1, 2, 3, 4, 5$) at distance $r_i(t)$ from the helicopter at time t is computed using Eq. (30),

$$L_i(t) = L_{\text{ref}}(\gamma(t), \Phi(t)) - \text{att}(r_i(t)) \text{ (dB)} \tag{31}$$

Let $L_m(t)$ be the average of the energies of these noise levels, and the energy-based noise estimation E_A can be computed as follows:

$$L_m(t) = 10 \log\left[\frac{1}{5}\sum_{i=1}^{5} 10^{\frac{L_i(t)}{10}}\right] \text{ (dB)} \tag{32}$$

$$E_A = \int_0^{t_f} 10^{\frac{L_m(t)}{10}}\, \mathrm{d}t \tag{33}$$

E_A is also expressed as follows:

$$E_A = \frac{1}{5}\sum_{i=1}^{5} E_{Ai} \tag{34}$$

$$E_{Ai} = \int_0^{t_f} 10^{\frac{L_i(t)}{10}}\, \mathrm{d}t \tag{35}$$

That is to say, in this paper, the energy-based noise estimation E_A was determined by averaging the energies of the noise at the measurement points. Note that $10^{L_m(t)/10}$ and $10^{L_i(t)/10}$ are dimensionless quantities and E_A has a unit of time. E_A was minimized in this study.

However, if we were to minimize only E_A as a performance index, the optimal thrust T, which is a control value, would cause chattering phenomena between the upper bound and lower bound, because the performance index does not include the control variables implicitly, and the equations of motion, Eqs. (1–6), are linear forms with respect to the thrust T [12]. To prevent the chattering, the square integration of the variation of the control values from $T/mg = 1$ and $\Theta = \Phi = 0$ in steady level flight was also minimized:

$$S_u = \int_0^{t_f} \left\{\left(\frac{T}{mg} - 1\right)^2 + \Theta^2 + \Phi^2\right\} \mathrm{d}t \tag{36}$$

Thus, the performance index minimized in this study is defined as

$$J = E_A + wS_u \tag{37}$$

The weight factor w was empirically determined to be 2.0×10^6. Here, the units of pitch angle Θ and roll angle Φ are radians and S_u has the same unit as E_A. The value of the weight factor is a nearly minimum value within a range where both the undesired oscillation of the thrust and increase in the original index E_A are small.

E. Two Cases of Computational Optimization

For the problem defined previously, the constraint conditions were set according to two cases below, and the computational optimization was performed.

Case 1: The upper limit on the climb rate was set to be 800 ft/ min in Eqs. (20) and (21).

Case 2: To avoid ascent flight, the upper limit on the climb rate in Eqs. (20) and (21) was changed to Eq. (22).

The reason the upper limit on the climb rate in case 2 was changed is that we foresaw that the suppression of ground-level noise would result in an optimal solution in which the helicopter ascended and flew at a high altitude. Thus, the climb rate was constrained to obtain a flight close to a conventional landing approach. Moreover, for both of these cases, the optimal solutions were computed by substituting a value between −20 and 20 kt for the wind speed u_g and 31.34 and −58.66 deg for the wind direction ψ_g. These angles are parallel and perpendicular to the direction from the terminal point to the initial point, respectively. Because the vehicle is blown in wind conditions, it is hard for the pilot to follow the trajectories that are optimized in the cases of no wind. This is why the wind effect on the optimal trajectories was investigated.

The computational optimization was conducted with the helicopter model, constraint conditions, noise source model, propagation model, and performance index described previously. The computational optimization was performed using the block-diagonal Hessian (BDH) method [9], which can incorporate all kinds of constraint conditions and demonstrates excellent convergence. This method discretizes all of the state variables, the control variables, motion equations, and constraint condition equations, which are functions of time, and transforms the optimal control problem, which is a dynamic-optimization problem, into a nonlinear programming problem that is a static-optimization problem. An optimal solution to the converted nonlinear programming problem was computed using the sequential quadratic programming (SQP) method. A feature of the BDH method is to discretize the motion equations with the trapezoidal rule. The discretization makes the Hessian in the SQP method a sparse block-diagonal matrix and allows an efficient computation. The number of nodes of the discretization was 100; hence, the numbers of optimization variables and equality–inequality constraints were, respectively, about 900 and 1500.

F. Computational Optimization Results

The results of the computational optimization without wind, $u_g = 0$, are shown in Figs. 5–12 and Table 2. The noise model used in the study generated a large noise in the range −15 to 5 deg of the flight path angle, with its maximum at about −5 deg. If the helicopter flew straight from the initial point to the terminal point, it would fly at such a flight path angle near measurement points 1, 3, and 5. Optimal solutions therefore attempt to avoid this flight path angle and the measurement points. In addition, because the performance index includes the time integral of the noise, the flight time is likely to be shortened. As shown in Fig. 5, the horizontal flight paths of the two cases roughly correspond. The path heads for the runway while turning to avoid the noise measurement points on the ground.

In the problem setting of case 1, the optimized initial altitude is 1850 ft. A straight descent flight from this altitude toward the terminal point would be necessary to fly at the flight path angle that

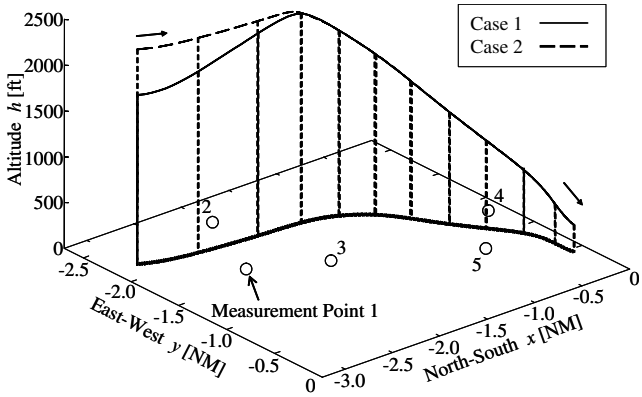

Fig. 5 Optimal trajectories.

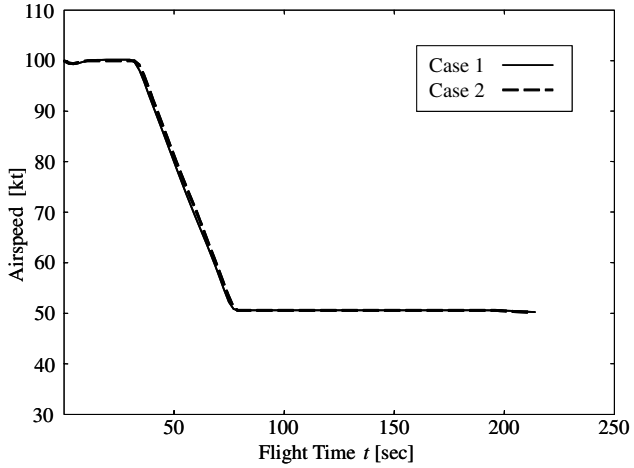

Fig. 6 Optimal airspeed histories.

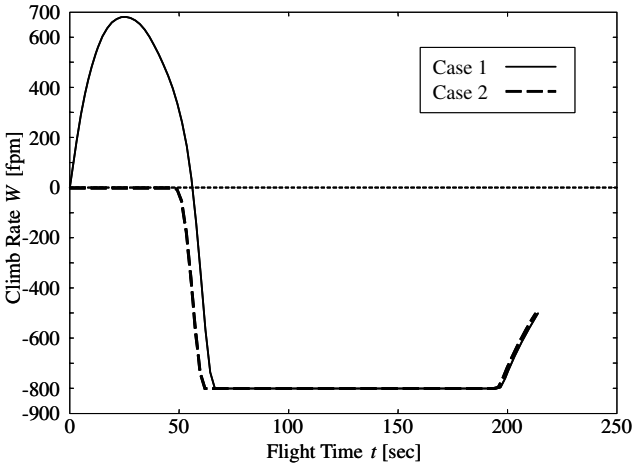

Fig. 7 Optimal climb-rate histories. (fpm = ft/min.)

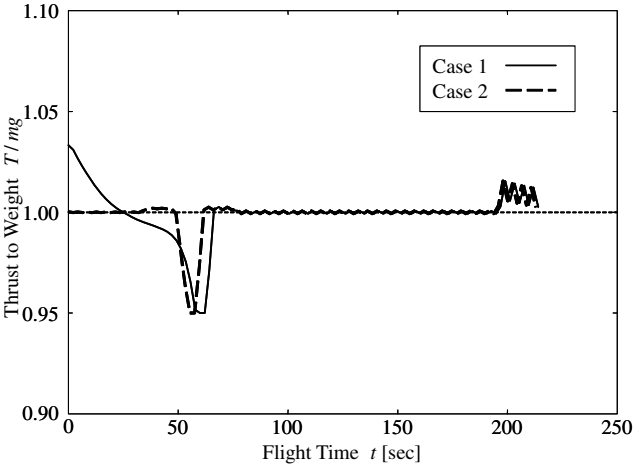

Fig. 8 Optimal thrust-to-weight histories.

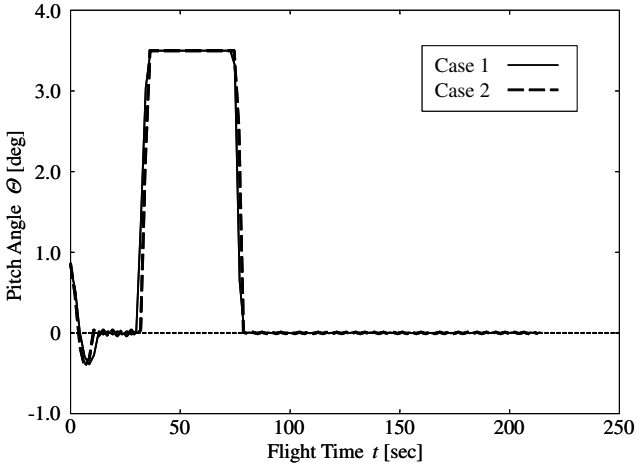

Fig. 9 Optimal pitch angle histories.

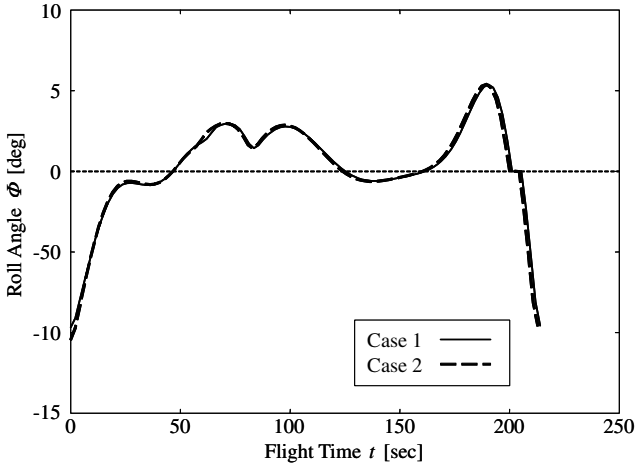

Fig. 10 Optimal roll angle histories.

increases the noise. For this reason, in the optimal solution, there is a moment of ascent after the flight begins. The climb rate and flight path angle at this time are about 600 ft/min and 4 deg, respectively. The helicopter starts to descend at the maximum descent rate (800 ft/min) just after reaching an altitude of 2300 ft. When the ascent changes to the descent, the flight path angle passes through the vicinity of -5 deg as quickly as possible to avoid loud noise. If the descent rate was 800 ft/min and the horizontal velocity was 100 kt, which was the initial velocity, the flight path angle would be -4.5 deg, which would cause a loud noise. Thus, the helicopter decreases the horizontal velocity to the minimum velocity of 50 kt before the descent flight. This allows the steeper descent at a flight path angle of -9.0 deg. Because a shorter flight time decreases the performance function, the helicopter flies at an initial velocity of 100 kt for a while after the flight begins, and then it increases the pitch angle and decreases the velocity at the maximum deceleration of Eqs. (23) and (24). In the latter half of the flight, the helicopter descends at the maximum sink rate, which is more severe at a lower altitude, to avoid producing a loud noise. The flight changes from the ascent to the descent when the descending flight leads exactly to the terminal point.

In case 2, to obtain a flight path similar to a normal approach, the computational optimization with the constraint condition preventing an ascent flight was conducted. The optimized initial altitude turned out to be 2271 ft. The horizontal velocity remains 100 kt after the flight begins, but soon decreases, and the helicopter begins the steepest descent at a horizontal velocity of 50 kt. Because the flight time is decreased, the helicopter does not decelerate as soon as the flight begins, similar to case 1. The descent trajectory is exactly the same as in case 1.

Figures 11 and 12 indicate the noise levels at the measurement points for cases 1 and 2 (without wind). When the helicopter passes over each measurement point, a loud noise is measured. In addition, the shallow flight path at a low altitude near the terminal point brings the flight path angle close to the angle at which the large noise occurs, and the measured noise increases. Moreover, the noise increases temporally around 60 s because the flight path angle in transition to the descent flight passes the angle yielding the largest noise. Even

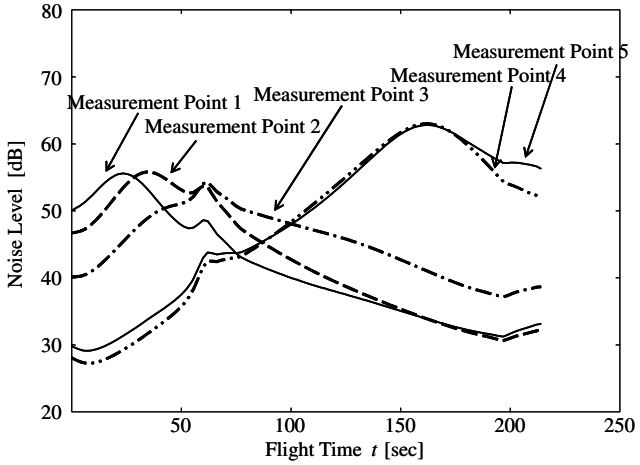

Fig. 11 Noise levels according to the optimal solution (case 1).

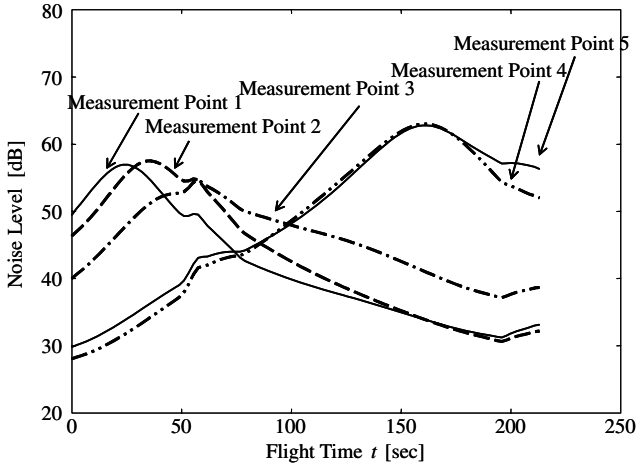

Fig. 12 Noise levels according to the optimal solution (case 2).

though the flight altitude of case 2 is higher than that of case 1, there is not a great difference between the noises. These findings show that the influence of the flight altitude on the noise is not particularly large in this study, but rather the influence of the flight path angle is dominant.

Table 2 shows the energy-based noise estimation E_A, which is a primary factor of the performance index, the penalty term for control variations S_u in Eq. (36), flight time t_f, and temporal-mean noise level L_A. This temporal-mean noise level is a quantity expressing the time averaging of the energy-based noise estimation E_A. That is to say, it is calculated as

$$L_A = 10\log\left(\frac{E_A}{t_f}\right) = 10\log\left(\frac{1}{t_f}\int_0^{t_f} 10^{\frac{L_m(t)}{10}}\,\mathrm{d}t\right)\ (\mathrm{dB}) \qquad (38)$$

The table indicates that, though the flight time is longer in case 1 than in case 2, the energy-based noise estimation E_A of case 1 is smaller than that of case 2, and thus the noise level L_A of case 1 is also smaller. This means that the noise level has a higher dependence on the flight path angle than on the flight altitude. However, the difference in the noise levels of the two cases is not particularly large.

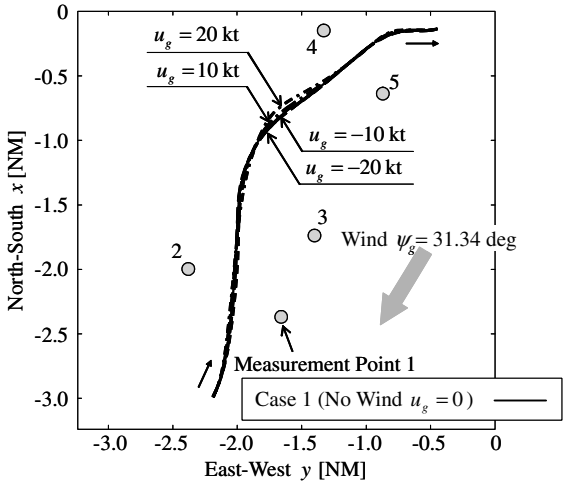

Fig. 13 Horizontal flight paths of the optimal trajectories (case 1 with the wind $\psi_g = 31.34$ deg).

Next, this paper considers case 1 with wind to examine the influence of wind on the optimal solutions. Hereafter, the initial altitude is fixed, which is not specified in case 1, to be the optimal altitude of 1850 ft to compare the optimal solutions under wind and no-wind conditions. A value between −20 and 20 kt is substituted for the wind speed u_g, and 31.34 or −58.66 deg is substituted for the wind direction ψ_g. It should be noted that the wind only impacts the flight performance and not noise propagation. Figures 13–16 show the optimal flight trajectories with a wind direction ψ_g of 31.34 deg. Because the wind direction is almost parallel to the flight azimuth, the flight path in the horizontal plane hardly changes with the wind speed, as shown in Fig. 13. Though Fig. 14 shows that the vertical trajectories change greatly, the features of the trajectories in the vertical plane are the same as in the case of no wind; the optimal trajectory is based on the ascent and descent flight. The noise depends on the flight path angle referenced to airspeed, rather than ground speed. For example, as shown in Fig. 16, which indicates the flight path angle referenced to ground speed, the helicopter flying against the wind descends with a steep path to reduce the noise. In contrast, the flight path angles referenced to the airspeeds are roughly the same in every case. This result is an effect of the wind parallel to the flight azimuth on the optimal trajectory.

On the other hand, Figs. 17–20 show the optimal flight trajectories with a wind direction ψ_g of −58.66 deg; that is, the wind is almost perpendicular to the flight azimuth. Figures 18 and 19 indicate that the optimal trajectory in the vertical plane hardly changes with the wind speed. In addition, there is no large change in the flight paths in the horizontal plane either. It is probable that there is only one horizontal path that minimizes the noise level on the ground with or without the wind. Figure 20 shows that the vehicle floating with the cross wind changes its roll angle to follow such a trajectory, depending on the wind speed.

IV. Flight Experiments

A. Flight Experiment Method

To confirm the optimal control results, we flew the optimal flight trajectories and compared the real flights with the simulations. The optimal solutions obtained earlier in this paper differ from the usual conventional approaches taken by pilots. Before conducting flight experiments, the tracking of the optimal solutions is confirmed using a flight simulator. As a result, one pilot commented that adequate

Table 2 Comparison of optimal solutions

	Energy-based noise estimation E_A, s	Penalty term for control variations S_u, s	Flight time t_f, s	Temporal-mean noise level L_A, dB
Case 1	4.45×10^7	1.03	213.9	53.2
Case 2	4.68×10^7	0.89	212.9	53.4

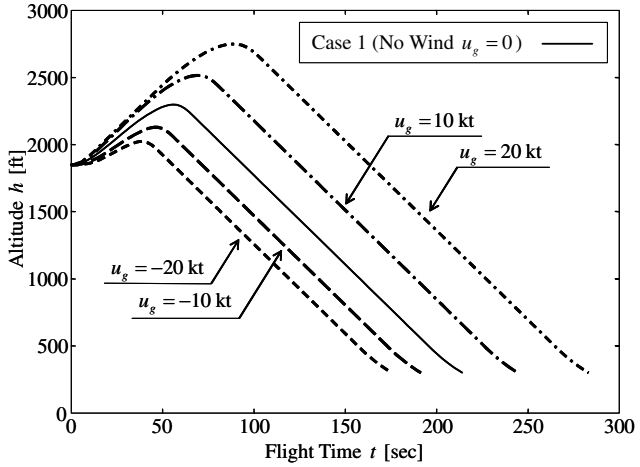

Fig. 14 Optimal altitude histories (case 1 with the wind $\psi_g = 31.34$ deg).

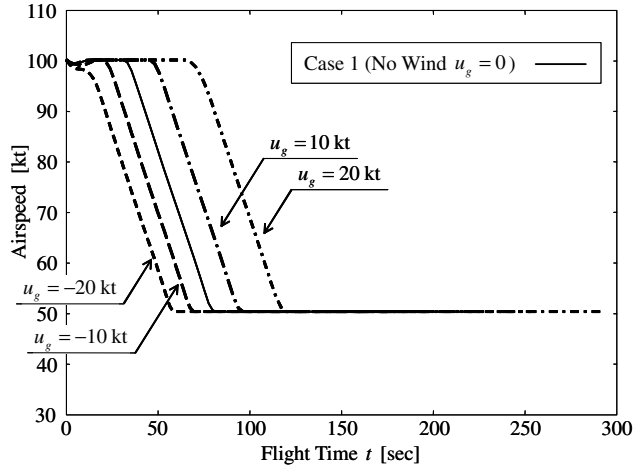

Fig. 15 Optimal airspeed histories (case 1 with the wind $\psi_g = 31.34$ deg).

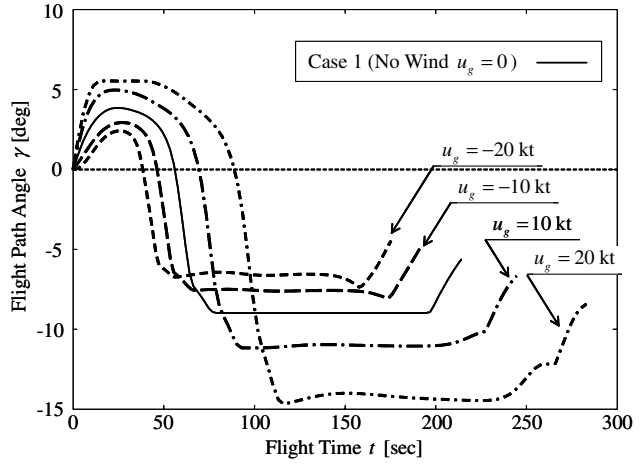

Fig. 16 Optimal flight path angle histories (case 1 with the wind $\psi_g = 31.34$ deg).

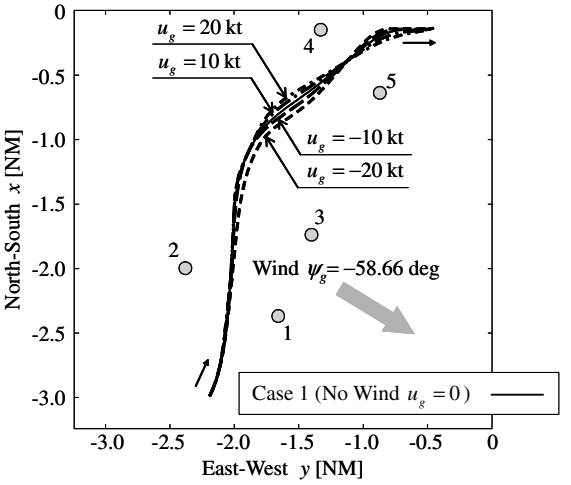

Fig. 17 Horizontal flight paths of the optimal trajectories (case 1 with the wind $\psi_g = -58.66$ deg).

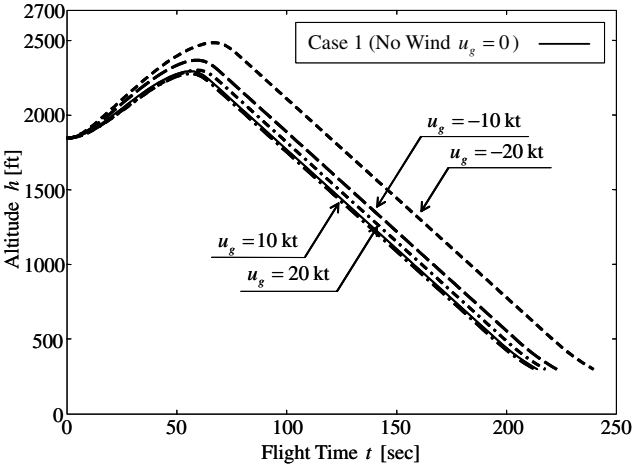

Fig. 18 Optimal altitude histories (case 1 with the wind $\psi_g = -58.66$ deg).

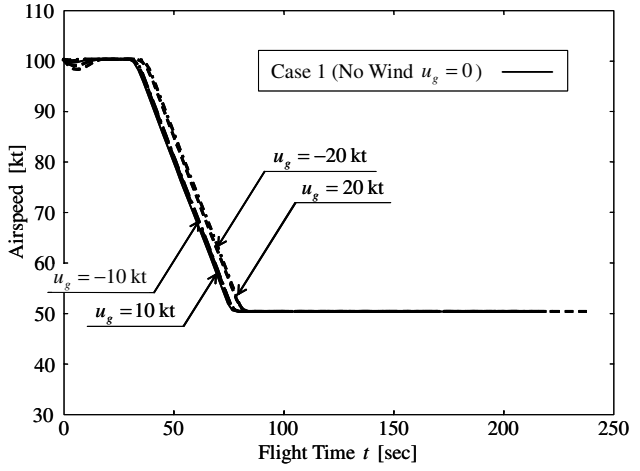

Fig. 19 Optimal airspeed histories (case 1 with the wind $\psi_g = -58.66$ deg).

acquaintance with the timing of the altitude transition made it possible to track the optimal solutions.

As stated previously, flight experiments were performed at the Taiki multipurpose aeronautical park using the JAXA-owned MuPAL-ε. The pilot controlled all flights manually. To facilitate the tracking of the optimal solutions, the flight history was indicated using an experimental display (Fig. 21) [13], which is called "tunnel in the sky," installed on an instrument panel. This display indicated the flight trajectory with speed commands that the pilot used for the tracking information. Noise levels were recorded at the five measurement points on the ground using noise measurement devices

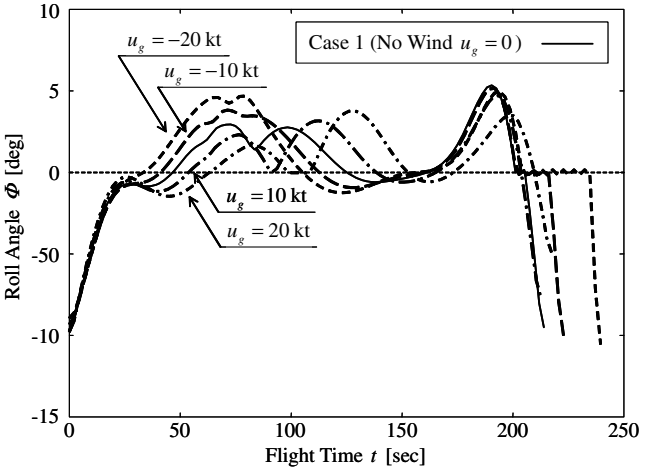

Fig. 20 Optimal roll angle histories (case 1 with the wind $\psi_g = -58.66$ deg).

Fig. 21 Experimental display panel ("tunnel-in-the-sky" display).

as shown in Fig. 22. In the flight experiments, a normal landing approach was also used in addition to the two cases of the optimal flights described in the previous section. Because the wind during the flight experiment was weak and its influence was considered to be small, the optimal solutions with $u_g = 0$ were used as the flight tracking objectives. The numerical optimal solutions with $u_g = 0$ and the results of the flight experiments are compared.

B. Flight Experiment Results

The flight data obtained using MuPAL-ε's measurement systems for each flight case are shown in Figs. 23–25. A comparison of these with the data in Figs. 5–7 suggests that, because the overall tracking of the optimal solutions is precise, the constraint conditions of the computational optimization in Eqs. (19–25) are defined appropriately. The flight times are shorter in the experiments than in the optimal solutions, and the sink rates are larger in the experiments. This finding suggests that, although we judged that there was no wind when the experiments were conducted, a slight following wind may in fact have existed. Although the pilot made an effort to follow the indicated trajectory and airspeed, the airspeed and climb rate had vibrations with the amplitudes of about 5 and 2 m/s, respectively, due to the wind effect and deceleration delay. As long as the pilot flies manually, such errors are inevitable. For computational optimization in the future, it will probably be necessary to determine an optimal solution (a robust optimal solution) that suppresses the additional noise level that occurs due to tracking errors. According to the pilot, it

Fig. 22 A noise measurement device.

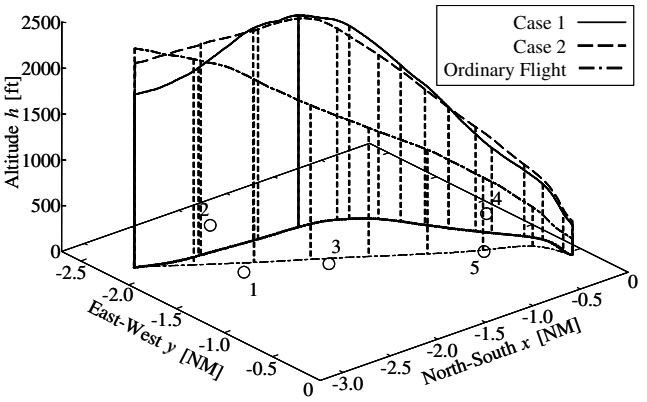

Fig. 23 Experimental result (trajectories).

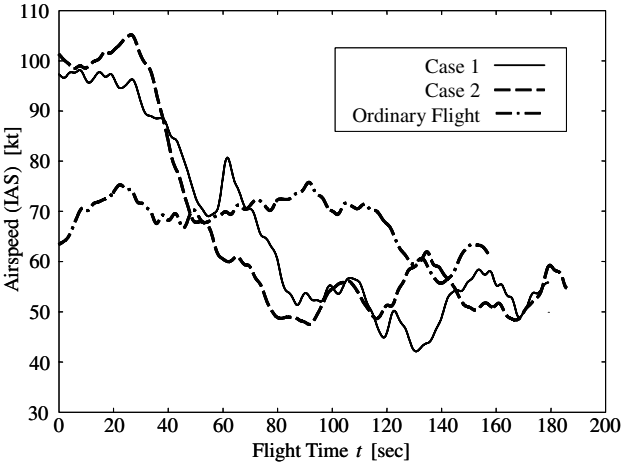

Fig. 24 Experimental result (airspeed histories).

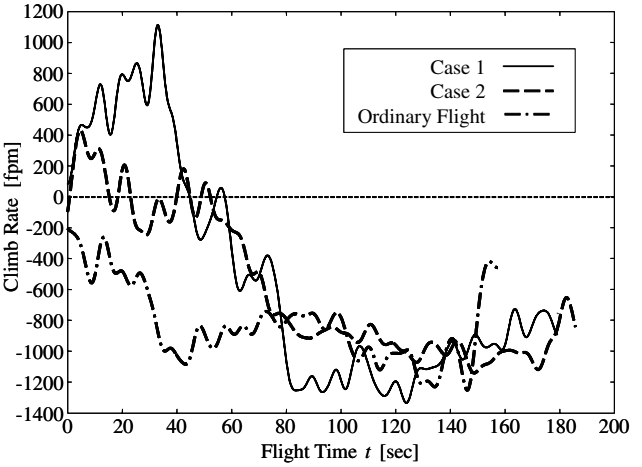

Fig. 25 Experimental result (climb-rate histories).

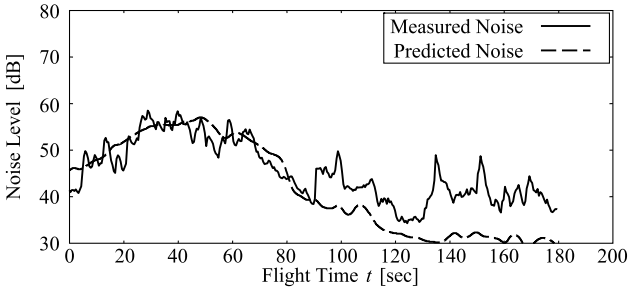

a) Measurement point 2

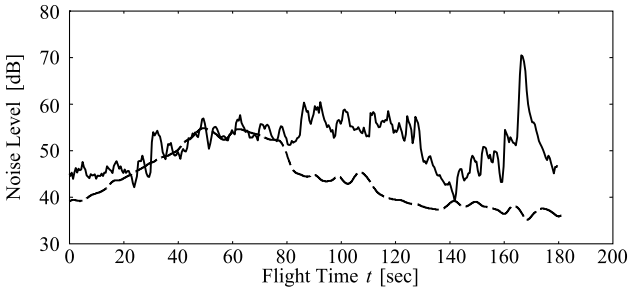

b) Measurement point 3

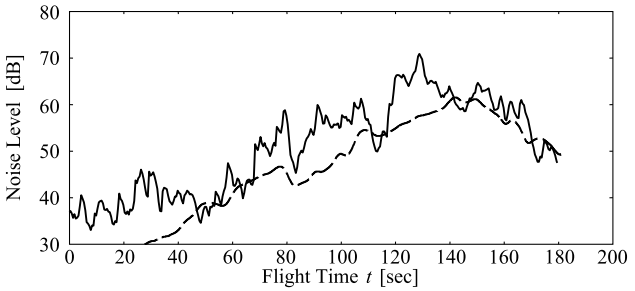

c) Measurement point 4

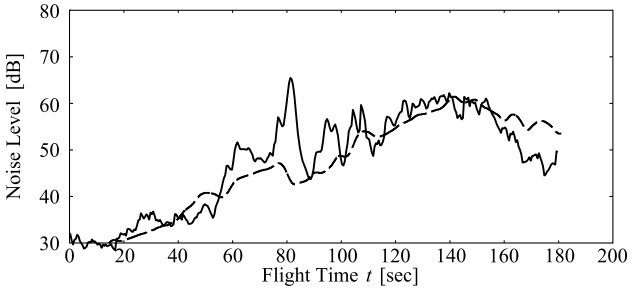

d) Measurement point 5

Fig. 26 Noise levels according to the flight experiment (case 1).

was difficult to match the airspeed and climb rate perfectly because he was confused regarding the timing of their changes, but it was not difficult to make the vehicle position track the optimal solution.

A landing approach that the pilot judged to be common was also conducted in the flight experiments to compare it with the optimal flights. This approach is indicated as the normal approach in Figs. 23–25. In the normal approach, the helicopter descended straight toward the terminal point at a constant airspeed and flight path angle before the heading angle was adjusted near the runway. In general, the pilot did not change the vehicle's attitude positively so as to be able to pay attention to the surroundings in addition to the maneuvering operation.

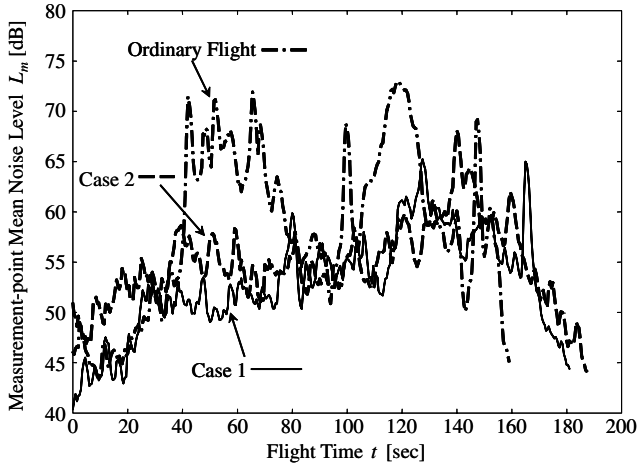

Fig. 27 Measurement-point mean noise level according to the flight experiment.

As an example, Fig. 26 shows the noise levels actually recorded at the measurement points for case 1. The instrument at measurement point 1 was out of order; the four noise levels at measurement points 2–5 are indicated in this figure. The figure shows the noise levels predicted from the flight data, the noise source model, and the attenuation model as well as the actually measured noise levels. A comparison between the measured noise levels and the predicted noise levels reveals the precision of the noise source and attenuation models. The predicted levels tended to correspond with the measured levels, especially when the noise levels were high. The noise levels could be predicted within about 5 dB error except for spikelike noises, which may emanate from cars passing near the measurement points. However, even when little noise was predicted because the vehicle and the measurement point were far apart, a noise of about 40 dB was often measured. This is due to background noise. It is very difficult to isolate the helicopter noise within the measured noise. To improve the accuracy of the noise estimation, the measurement points should be set where noises other than the helicopter noise are minimal. Figure 27 shows measurement-point mean noise levels in the flight experiments. The noise levels of cases 1 and 2 were lower than that of the normal approach. The former levels were as much as 10 dB lower than the latter level. Next, let us compare the measured noise level with those of the optimal solutions in Figs. 11 and 12. The overall trends of the measured noise levels are well accorded with those predicted by the optimal solutions, but there is a maximum error of around 10 dB at each measurement point.

Table 3 summarizes the results of the flight experiments and the optimal solutions. Because the noise at measurement point 1 was not measured, the energy-based noise estimations and temporal-mean noise levels of the optimal solutions were recalculated without including measurement point 1 so as to compare both noise levels under the same conditions; hence these values are different from those in Table 2. The energy-based noise estimations calculated in the flight experiments are larger than those of the optimal solutions. The temporal-mean noise levels calculated from the energy-based

Table 3 Comparison of the optimal solutions and flight experimental results (the energy-based noise estimations and temporal-mean noise levels were computed without measurement point 1)

	Energy-based noise estimation E_A, s		Flight time t_f, s		Temporal-mean noise level L_A, dB	
	Optimal solution	Flight experiment	Optimal solution	Flight experiment	Optimal solution	Flight experiment
Case 1	5.25×10^7	6.85×10^7	213.9	181.2	53.9	55.7
Case 2	5.44×10^7	1.60×10^8	212.9	187.2	54.1	59.3
Normal approach		5.77×10^8	——	159.2	——	65.6

noise estimations and the flight times in cases 1 and 2 were 1.8 and 5.2 dB larger than those of the optimal solutions, respectively. The difference between cases 1 and 2 in the flight experiments is larger than in the optimal solutions. In particular, the noise level in case 2 is significantly different. This is because of the errors of the noise source and attenuation models, the tracking errors of the flight trajectory and airspeed, and the background noise emanating from noise sources other than the helicopter. However, the noise level in case 1 was lower than in case 2; the magnitude relation of the two cases in the flight experiments was equal to that in the optimal solutions. In the normal approach, the pilot chose the straight trajectory to the terminal point, which made the flight time of the normal approach the shortest. However, the helicopter approached the measurement points, and the temporal-mean noise level of the normal approach was larger than those of the optimal solutions. The noise level was greatly different from those in the optimal trajectories where the helicopter avoided the measurement points. This study confirmed that the optimization of the three-dimensional trajectory can decrease the ground noise.

V. Conclusions

This study determined the flight profiles of the helicopter landing approach that minimized the ground-level noise using computational optimization. The optimal solutions attempted to avoid the flight path angle that caused the most noise as well as the measurement points at which the noise levels should be minimized. The paths in the horizontal plane of the optimal flights were almost the same regardless of the initial condition and the wind; the helicopter flew away from the measurement points. In contrast, the flights in the vertical plane tended to avoid the flight path angle at which the blade-vortex interaction noise, the largest noise source, increased by adjusting the airspeed and climb rate. The sink rate in the latter part of the optimal flights was higher than in the normal approach. Furthermore, flight experiments on the basis of the optimal solutions were conducted. The results show a difference of approximately 5 dB between the predicted noise level and the actually measured noise level because of the background noise and tracking error in the real environment. However, the tendency of the actually measured noise levels is in excellent agreement with that of the predicted noise levels, and the noise of the optimal flights decreased in comparison with the conventional flight.

Acknowledgment

This research was carried out as a collaboration between the University of Tokyo and the Japan Aerospace Exploration Agency (JAXA).

References

[1] Conner, D. A., Edwards, B. D., Decker, W. A., Marcolini, M. A., and Klein, P. D., "NASA/ARMY/BELL XV-15 Tiltrotor Low Noise Terminal Area Operations Flight Research Program," AIAA Paper 2000-1923, 2000.

[2] Xue, M., and Atkins, E. M., "Noise-Minimum Runway-Independent Aircraft Approach Design for Baltimore-Washington International Airport," *Journal of Aircraft*, Vol. 43, No. 1, 2006, pp. 39–51. doi:10.2514/1.15692

[3] Yin, J., and Buchholz, H., "Toward Noise Abatement Flight Procedure Design: DLR Rotorcraft Noise Ground Footprints Model," *Journal of the American Helicopter Society*, Vol. 52, No. 2, 2007, pp. 90–98.

[4] Vormer, F. J., Mulder, M., Van Paassen, M. M., and Mulder, J. A., "Optimization of Flexible Approach Trajectories Using a Genetic Algorithm," *Journal of Aircraft*, Vol. 43, No. 4, 2006, pp. 941–952. doi:10.2514/1.13609

[5] Ishii, H., Gomi, H., Okuno, Y., Uchida, J., and Tsuchiya, T., "Flight Tests of Helicopter Noise Abatement Operations," AIDAA (Associazione Italiana di Aeronautica e Astronautica) and Agusta Paper 28, 2005.

[6] Ishii, H., Okuno, Y., and Funabiki, K., "Flight Experiments for Aircraft Noise Measurement Using Tunnel-in-the-Sky Display," AIAA Paper 2002-4880, 2002.

[7] Ishii, H., Gomi, H., and Okuno, Y., "Helicopter Flight Tests for BVI Noise Measurement Using an Onboard External Microphone," AIAA Paper 2005-6119, 2005.

[8] Ochi, A., Aoyama, T., Saito, S., Shima, E., and Yamakawa, E., "BVI Noise Predictions by Moving Overlapped Grid Method," *AHS 55th Annual National Forum*, The American Helicopter Society, Alexandria, VA, 1999, pp. 1400–1413.

[9] Yokoyama, N., Suzuki, S., and Tsuchiya, T., "Convergence Acceleration of Direct Trajectory Optimization Using Novel Hessian Calculation Methods," *Journal of Optimization Theory and Applications*, Vol. 136, No. 3, 2008, pp. 297–319. doi:10.1007/s10957-008-9351-0

[10] Tsuchiya, T., Ishii, H., Uchida, J., Gomi, H., Matayoshi, N., and Okuno, Y., "Optimal Flight for Ground Noise Reduction in Helicopter's Landing Approach: Optimal Altitude and Velocity Control," *Transactions of the Japan Society for Aeronautical and Space Sciences*, Vol. 50, No. 169, 2007, pp. 209–217. doi:10.2322/tjsass.50.209

[11] Yoshioka, H., Iwasaki, K., and Yamada, I., "Recent Development on Energy-Based Aircraft Noise Modeling in Japan," *18th International Congress on Acoustics* [CD-ROM], 2004.

[12] Bryson, A. E., Jr., and Ho, Y. C., *Applied Optimal Control*, Hemisphere Publishing Company, New York, 1975.

[13] Funabiki, K., "Design of Tunnel-in-the-Sky Display and Curved Trajectory," ICAS Paper 2004-8.4.4, 2004.